Inorganic Chemistry
Article

Inorg. Chem. **2010**, *49*, 4949–4959 **4949**
DOI: 10.1021/ic100050r

Cobalt, Manganese, Nickel, and Vanadium Derivatives of the Cyclic 48-Tungsto-8-Phosphate $[H_7P_8W_{48}O_{184}]^{33-}$

Bassem S. Bassil,[†] Masooma Ibrahim,[†] Sib Sankar Mal,[†,∥] Andreas Suchopar,[†] Rosa Ngo Biboum,[‡] Bineta Keita,*[,‡] Louis Nadjo,[‡] Saritha Nellutla,[§,⊥] Johan van Tol,[§] Naresh S. Dalal,*[,§] and Ulrich Kortz*[,†]

[†]*Jacobs University, School of Engineering and Science, P.O. Box 750 561, 28725 Bremen, Germany,* [‡]*Laboratoire de Chimie Physique, UMR 8000 CNRS, Université Paris-Sud 11, 91405 Orsay Cedex, France, and* [§]*Department of Chemistry and Biochemistry, Florida State University and Center for Interdisciplinary Magnetic Resonance, National High Magnetic Field Laboratory, Tallahassee, Florida 32306−4390.* [∥]*Current address: Center For Catalysis Research and Innovation, Department of Chemistry, University of Ottawa, 10 Marie Curie, K1N 6N5, ON, Canada.* [⊥]*Current address: Department of Chemistry, North Carolina State University, Raleigh, NC 27695-8204.*

Received January 8, 2010

The cobalt(II) containing tungstophosphate $[Co_4(H_2O)_{16}P_8W_{48}O_{184}]^{32-}$ (**1**) has been synthesized by addition of Co^{2+} ions to an aqueous solution of $[H_7P_8W_{48}O_{184}]^{33-}$ (**P_8W_{48}**) and characterized by single-crystal XRD, IR, and UV−vis spectroscopy, elemental analysis, electrochemistry, and magnetochemistry. The novel polyanion **1** is a derivative of the superlacunary **P_8W_{48}** with four cobalt(II) ions coordinated to the rim of the central cavity and two additional cobalt(II) ions linked on the outside bridging neighboring polyanions. Using similar synthetic procedures, but adding a few drops of H_2O_2, we isolated the manganese(II) derivative $[Mn_4(H_2O)_{16}(P_8W_{48}O_{184})(WO_2(H_2O)_2)_2]^{28-}$ (**2**) and its nickel(II) analogue $[Ni_4(H_2O)_{16}(P_8W_{48}O_{184})(WO_2(H_2O)_2)_2]^{28-}$ (**3**). Both polyanions have picked up two equivalents of tungsten resulting in the unprecedented $\{P_8W_{50}\}$ host framework. We also made the vanadium(V) derivative $[(VO_2)_4(P_8W_{48}O_{184})]^{36-}$ (**4**), with four tetrahedral vanadate groups grafted to the **P_8W_{48}** host. The voltammetric patterns associated with the W-centers in polyanions **1**, **2**, and **4** display enough distinct features allowing for a qualitative classification according to relative basicity of the reduced polyanions: **2** > **P_8W_{48}** > **1** > **4**. The electrochemistry of **1** offers a new example for detection of the Co^{2+} centers in a multicobalt containing polyanion. During a study of the Mn^{2+} centers of **2** at pH 5, a film deposition is observed. The vanadium(V) centers of **4** are well-behaved in a pH 0.33 medium. Temperature and magnetic field dependence of the magnetic moment of **1**−**3** were performed on a SQUID magnetometer over the temperature range 1.8−250 K and field range 0−7 T. The results are consistent with the model of noninteracting 3d metal ions. Variable temperature (4−295 K) and variable frequency (34−413 GHz) EPR measurements support the magnetic susceptibility results. The zero-field splitting *D* and *g* values obtained for **1**−**3** are in agreement with those reported for high-spin Co^{2+}, Mn^{2+}, and Ni^{2+} ions in axially distorted octahedral environments.

Introduction

Early transition metals such as vanadium, molybdenum, or tungsten in high oxidation states are able to form metal−oxygen cluster anions, commonly referred to as polyoxoanions or polyoxometalates (POMs).[1] Transition metal substituted POMs are a rapidly growing field because of their potential applications in areas as diverse as magnetochemistry, catalysis, medicinal chemistry, material science, and nanotechnology.[2] POMs exhibit a variety of tunable properties, including molecular composition, size, shape, charge density, redox potentials, acidity, and solubility. Generally, POMs are

*To whom correspondence should be addressed. E-mail: bineta.keita@u-psud.fr. Fax: (+33)-1-69154328 (B.K.). E-mail: dalal@chemmail.chem.fsu.edu. Fax: (+1)850-644 3398 (N.S.D.). E-mail: u.kortz@jacobs-university.de. Fax: +49-421-200 3229 (U.K.).

(1) (a) Pope, M. T.; Müller, A. *Angew. Chem., Int. Ed. Engl.* **1991**, *30*, 34. (b) Pope, M. T. *Heteropoly and Isopoly Oxometalates*; Springer: Berlin, 1983. (c) Souchay, P. *Polyanions et Polycations*; Gauthier-Villars: Paris, 1963.

(2) (a) *Polyoxometalates: from Platonic Solids to Anti Retroviral Activity*; Pope, M. T., Müller, A., Eds.; Kluwer: Dordrecht, 1994. (b) *Chem. Rev.* **1998**, *98*, 1−389; special thematic issue on polyoxometalates. (c) *Polyoxometalate Chemistry: From Topology via Self-Assembly to Applications*; Pope, M. T., Müller, A., Eds.; Kluwer: Dordrecht, 2001. (d) *Polyoxometalate Chemistry for Nano-Composite Design*; Yamase, T., Pope, M. T., Eds.; Kluwer: Dordrecht, 2002. (e) Cronin, L. In *Comprehensive Coordination Chemistry II*; McCleverty, J. A., Meyer, T. J., Eds.; Elsevier: Amsterdam, 2004; Vol. *7*, pp 1−57. (f) Hasenknopf, B. *Front. Biosc.* **2005**, *10*, 275. (g) Proust, A.; Thouvenot, R.; Gouzerh, P. *Chem. Commun.* **2008**, 1837. (h) Kortz, U.; Müller, A.; van Slageren, J.; Schnack, J.; Dalal, N. S.; Dressel, M. *Coord. Chem. Rev.* **2009**, *253*, 2315. (i) Kortz, U., Ed. *Eur. J. Inorg. Chem.* **2009**, *34*; special thematic issue on polyoxometalates.

Published on Web 04/26/2010

formed via condensation reactions, but the detailed formation mechanism is still largely unexplored and usually referred to as self-assembly. Although the first POMs were reported by Berzelius almost 200 years ago, they continue to display unprecedented structures and compositions associated with unexpected properties.

POMs can be subdivided into iso- and heteropolyanions, and in both cases, tungsten is the dominating addenda element leading to the large class of polytungstates. Heteropolytungstates with the hetero element phosphorus are most abundant, and the structures of these tungstophosphates are usually based on lacunary fragments of the Keggin ($[PW_{12}O_{40}]^{3-}$) or Wells−Dawson ion ($[P_2W_{18}O_{62}]^{6-}$), such as $[PW_{11}O_{39}]^{7-}$, $[PW_9O_{34}]^{9-}$, $[P_2W_{17}O_{61}]^{10-}$, and $[P_2W_{15}O_{56}]^{12-}$.[1b]

Only recently, the chemistry of the large, cyclic 48-tungsto-8-phosphate $[H_7P_8W_{48}O_{184}]^{33-}$ (**P_8W_{48}**) has been explored, although this polyanion had been reported already in 1985.[3] In 2005, our group prepared the 20-copper(II) containing $[Cu_{20}Cl(OH)_{24}(H_2O)_{12}(P_8W_{48}O_{184})]^{25-}$, which has been used for a variety of physicochemical studies ever since.[4] Very recently, we also reported two isostructural analogues of this ion with the central chloride guest replaced by bromide and iodide, $[Cu_{20}X(OH)_{24}(H_2O)_{12}(P_8W_{48}O_{184})]^{25-}$ (X = Br, I).[5] Mialane and co-workers have isolated the azide-derivative $[P_8W_{48}O_{184}Cu_{20}(N_3)_6(OH)_{18}]^{24-}$.[6] In addition, several other derivatives of **P_8W_{48}** are known including Pope's $\{Ln_4(H_2O)_{28}[K\subset P_8W_{48}O_{184}(H_4W_4O_{12})_2Ln_2(H_2O)_{10}]^{13-}\}_x$ (Ln = La, Ce, Pr, Nd),[7a] our $\{K(H_2O)\}_3\{Ru(p\text{-cymene})(H_2O)\}_4P_8W_{49}O_{186}(H_2O)_2]^{27-}$,[7b] Müller's/Pope's $[K_8\{P_8W_{48}O_{184}\}\{V^{V}_4V^{IV}_2O_{12}(H_2O)_2\}_2]^{24-}$,[7c] our/Müller's $[Fe_{16}(OH)_{28}(H_2O)_4P_8W_{48}O_{184}]^{20-}$,[7d] and Cronin's salts $K_{15}Li_5[Co_{10}(H_2O)_{34}(P_8W_{48}O_{184})]\cdot 54H_2O$, and $K_8Li_{12}[Co_{10}(H_2O)_{44}(P_8W_{48}O_{184})]\cdot 60H_2O$.[7e]

Some trimeric tungstophosphate ligands, based on three $\{P_2W_{12}\}$ units rather than four in **P_8W_{48}**, have also been reported recently. For example, we prepared a 36-tungsto-8-phosphate ligand based on three $\{P_2W_{12}\}$ units linked in a U-shape and incorporating two tetrameric uranyl-peroxo fragments, $[Li(H_2O)K_4(H_2O)_3\{(UO_2)_4(O_2)_4(H_2O)_2\}_2(PO_3OH)_2P_6W_{36}O_{136}]^{25-}$.[8] Very recently, Wang's group has discovered transition metal containing tungstophosphates based on the novel $\{P_6W_{39}\}$ type ligand, which can be considered as a trimeric, triangular derivative of **P_8W_{48}**.[9]

Here, we report on some novel cobalt(II), manganese(II), nickel(II) and vanadium(V) derivatives based on the **P_8W_{48}** wheel and the unprecedented $\{P_8W_{50}\}$ host framework.

Experimental Section

Synthesis. The wheel-shaped 48-tungsto-8-phosphate $[H_7P_8W_{48}O_{184}]^{33-}$ (**P_8W_{48}**) was synthesized according to the published procedure and identified by IR and ^{31}P NMR.[3] All other reagents were used as purchased without further purification.

$K_{12}Li_{16}Co_2[Co_4(H_2O)_{16}P_8W_{48}O_{184}]\cdot 60H_2O$ (KLi-1). A sample of $CoCl_2\cdot 6H_2O$ (0.079 g, 0.33 mmol) was dissolved in 1 M CH_3COOLi buffer solution (20 mL) at pH 5.3, and then $K_{28}Li_5[H_7P_8W_{48}O_{184}]\cdot 92H_2O$ (0.19 g, 0.013 mmol) was added. The solution was heated at 80 °C for 1 h and filtered hot. The filtrate was allowed to evaporate in an open beaker at room temperature. After 4−5 days, a dark pink crystalline product started to appear. Evaporation was allowed to continue at room temperature for two more weeks until the solution level approached the solid product, which was then collected by filtration and air-dried. Yield: 0.13 g (70%). IR: 1136(s), 1083(s), 1017(m), 931(sh), 911(sh), 793(s), 676(s), 525(w), 462(w) cm^{-1}. Elemental analysis calc (found): K 3.28 (3.27), Li 0.78 (0.63), W 61.63 (61.95), Co 2.47 (2.49), P 1.73 (1.53).

$K_{12}Li_{10}Mn_3[Mn_4(H_2O)_{16}(P_8W_{48}O_{184})(WO_2(H_2O)_2)_2]\cdot 67H_2O$ (KLi-2). A sample of $MnCl_2\cdot 4H_2O$ (0.065 g, 0.33 mmol) was dissolved in 2 M CH_3COOLi buffer solution (20 mL) at pH 4.0, and then $K_{28}Li_5[H_7P_8W_{48}O_{184}]\cdot 92H_2O$ (0.19 g, 0.013 mmol) was added. Then 6−10 drops of 30% H_2O_2 was added to this solution, which was heated at 80 °C for 1 h and filtered hot. The filtrate was allowed to evaporate in an open beaker at room temperature. After 2−3 days, a yellow crystalline product started to appear. Evaporation was allowed to continue at room temperature for 2 more weeks until the solution level approached the solid product, which was then collected by filtration and air-dried. Yield: 0.12 g (62%). IR: 1138(s), 1087(s), 1018(m), 982(sh), 930(sh), 920(sh), 800(s), 685(s), 572(w), 530(sh), 463(w) cm^{-1}. Elemental analysis calc (found): K 3.14 (3.26), Li 0.46 (0.43), Mn 2.57 (2.51), W 61.53 (61.73), P 1.66 (1.55).

$K_{14}Li_8Ni_3[Ni_4(H_2O)_{16}(P_8W_{48}O_{184})(WO_2(H_2O)_2)_2]\cdot 44H_2O$ (KLi-3). A sample of $NiCl_2\cdot 6H_2O$ (0.078 g, 0.33 mmol) was dissolved in 1 M CH_3COOLi buffer solution (20 mL) at pH 4.0, and then $K_{28}Li_5[H_7P_8W_{48}O_{184}]\cdot 92H_2O$ (0.19 g, 0.013 mmol) was added. Then 6−10 drops of 30% H_2O_2 was added to this solution, which was heated at 80 °C for 1 h and filtered hot. The filtrate was allowed to evaporate in an open beaker at room temperature. After 4−5 days, a green crystalline product started to appear. Evaporation was allowed to continue at room temperature for 2 more weeks until the solution level approached the solid product, which was then collected by filtration and air-dried. Yield: 0.13 g (69%). IR: 1139(s), 1088(s), 1020(m), 933(sh), 918(sh), 813(s), 685(s), 468(sh) cm^{-1}. Elemental analysis calc (found): K 3.75 (3.80), Li 0.38 (0.39), Ni 2.81 (2.76), W 62.90 (61.85), P 1.70 (1.60).

$K_{20}Li_{16}[(VO_2)_4(P_8W_{48}O_{184})]\cdot 48H_2O$ (KLi-4). A sample of $VOSO_4\cdot 5H_2O$ (0.035 g, 0.14 mmol) was dissolved in 1 M CH_3COOLi buffer solution (20 mL) at pH 5.3, and then $K_{28}Li_5[H_7P_8W_{48}O_{184}]\cdot 92H_2O$ (0.19 g, 0.013 mmol) was added. The solution was heated at 80 °C for 1 h and filtered hot. The filtrate was allowed to evaporate in an open beaker at room temperature. After one week, a brown crystalline product started to appear. Evaporation was allowed to continue at room

(3) (a) Contant, R.; Tézé, A. *Inorg. Chem.* **1985**, *24*, 4610. (b) Contant, R. *Inorg. Synth.* **1990**, *27*, 110.

(4) (a) Mal, S. S.; Kortz, U. *Angew. Chem. Int. Ed.* **2005**, *44*, 3777. (b) Jabbour, D.; Keita, B.; Nadjo, L.; Kortz, U.; Mal, S. S. *Electrochem. Commun.* **2005**, *7*, 841. (c) Alam, M. S.; Dremov, V.; Müller, P.; Postnikov, A. V.; Mal, S. S.; Hussain, F.; Kortz, U. *Inorg. Chem.* **2006**, *45*, 2866. (d) Liu, G.; Liu, T.; Mal, S. S.; Kortz, U. *J. Am. Chem. Soc.* **2006**, *128*, 10103. (e) Liu, G.; Liu, T.; Mal, S. S.; Kortz, U. *J. Am. Chem. Soc.* **2007**, *129*, 2408. (f) Chen, L.; Hu, J.; Mal, S. S.; Kortz, U.; Jaensch, H.; Mathys, G.; Richards, R. M. *Chem.—Eur. J.* **2009**, *15*, 7490. (g) Bao, Y.-Y.; Bi, L.-H.; Wu, L.-X.; Mal, S. S.; Kortz, U. *Langmuir* **2009**, *25*, 13000.

(5) Mal, S. S.; Bassil, B. S.; Ibrahim, M.; Nellutla, S.; van Tol, J.; Dalal, N. S.; Fernández, J. A.; López, X.; Poblet, J. M.; Ngo Biboum, R.; Keita, B.; Kortz, U. *Inorg. Chem.* **2009**, *48*, 11636.

(6) Pichon, C.; Mialane, P.; Dolbecq, A.; Marrot, J.; Rivière, E.; Keita, B.; Nadjo, L.; Sécheresse, F. *Inorg. Chem.* **2007**, *46*, 5292.

(7) (a) Zimmermann, M.; Belai, N.; Butcher, R. J.; Pope, M. T.; Chubarova, E. V.; Dickman, M. H.; Kortz, U. *Inorg. Chem.* **2007**, *46*, 1737. (b) Mal, S. S.; Nsouli, N. H.; Dickman, M. H.; Kortz, U. *Dalton Trans.* **2007**, 2627. (c) Müller, A.; Pope, M. T.; Todea, A. M.; Bögge, H.; van Slageren, J.; Dressel, M.; Gouzerh, P.; Thouvenot, R.; Tsukerblat, B.; Bell, A. *Angew. Chem., Int. Ed.* **2007**, *46*, 4477. (d) Mal, S. S.; Dickman, M. H.; Kortz, U.; Todea, A. M.; Merca, A.; Bögge, H.; Glaser, T.; Müller, A.; Nellutla, S.; Kaur, N.; van Tol, J.; Dalal, N. S.; Keita, B.; Nadjo, L. *Chem.—Eur. J.* **2008**, *14*, 1186. (e) Mitchell, S. G.; Gabb, D.; Ritchie, C.; Hazel, N.; Long, D.-L.; Cronin, L. *CrystEngComm* **2009**, *11*, 36.

(8) Mal, S. S.; Dickman, M. H.; Kortz, U. *Chem.—Eur. J.* **2008**, *14*, 9851.

(9) (a) Zhang, Z.-M.; Yao, S.; Li, Y.-G.; Wang, Y.-H.; Qi, Y.-F.; Wang, E.-B. *Chem. Commun.* **2008**, 1650. (b) Yao, S.; Zhang, Z.; Li, Y.; Lu, Y.; Wang, E.; Su, Z. *Cryst. Growth Des.* **2010**, *10*, 135.

Table 1. Crystal Data and Structure Refinement for **KLi-1**, **KLi-2**, **KLi-3**, and **KLi-4**

empirical formula	$K_{12}Li_{16}Co_2[Co_4(H_2O)_{16}$-$P_8W_{48}O_{184}]\cdot$ $60H_2O$ (**KLi-1**)	$K_{12}Li_{10}Mn_3[Mn_4(H_2O)_{16}$-$(P_8W_{48}O_{184})(WO_2(H_2O)_2)_2]\cdot$ $67H_2O$ (**KLi-2**)	$K_{14}Li_8Ni_3[Ni_4(H_2O)_{16}$-$(P_8W_{48}O_{184})(WO_2(H_2O)_2)_2]\cdot$ $44H_2O$ (**KLi-3**)	$K_{20}Li_{16}[(VO_2)_4$-$(P_8W_{48}O_{184})]\cdot$ $48H_2O$ (**KLi-4**)
MW	14319.6	14938.2	14614.9	14106.0
crystal system	triclinic	triclinic	triclinic	tetragonal
space group (no.)	$P\bar{1}$ (2)	$P\bar{1}$ (2)	$P\bar{1}$ (2)	$P4/m$ (83)
a/Å	15.9934(9)	15.7138(13)	15.8433(5)	24.0881(3)
b/Å	20.4843(15)	20.897(2)	20.3136(7)	24.0881(3)
c/Å	23.6382(14)	23.737(2)	24.2972(10)	21.7879(7)
α/deg	106.161(3)	108.898(3)	110.900(2)	90
β/deg	103.673(3)	97.269(3)	107.940(2)	90
γ/deg	95.424(3)	90.785(3)	94.935(2)	90
V/Å^3	7119.9(8)	7302.7(12)	6779.1(4)	12642.1(5)
Z	1	1	1	2
T/°C	−100	−100	−100	−100
λ/Å	0.71073	0.71073	0.71073	0.71073
D_c/mg m^{-3}	3.250	3.336	3.511	3.689
μ/mm^{-1}	20.001	20.150	21.674	22.395
$R[I < 2\sigma(I)]^a$	0.0687	0.0629	0.0577	0.0413
R_w (all data)^b	0.2321	0.1897	0.1722	0.1232

$^a R = \Sigma||F_o| - |F_c||/\Sigma|F_o|$. $^b R_w = [\Sigma w(F_o^2 - F_c^2)^2/\Sigma w(F_o^2)^2]^{1/2}$.

temperature for two more weeks until the solution level approached the solid product, which was then collected by filtration and air-dried. Yield: 0.13 g (71%). IR: 1141(s), 1090(s), 1021(m), 985(sh), 956(sh), 934(sh), 915(sh), 799(s), 697(s), 573(w), 526(sh), 465(w) cm^{-1}. Elemental analysis calc (found): K 5.54 (5.36), Li 0.79 (0.69), W 62.56 (60.25), V 1.44 (1.52), P 1.76 (1.82). NMR Data for **KLi-4**, ^{31}P NMR (D_2O): δ −8.1 ppm, ^{51}V NMR (D_2O): δ −559.4 ppm.

Elemental analyses were performed by Analytische Laboratorien, Lindlar, Germany. Infrared spectra were recorded on KBr pellets using a Nicolet Avatar spectrophotometer. All NMR spectra were recorded on a 400 MHz JEOL ECS instrument at room temperature using 5 mm tubes. The resonance frequencies for ^{31}P and ^{51}V NMR were 161.835 and 105.155 MHz, respectively, and the chemical shifts are reported with respect to 85% H_3PO_4 and neat $VOCl_3$, respectively.

X-ray Crystallography. Each crystal was mounted in a Hampton cryoloop using light oil for data collection at low temperature. Indexing and data collection were performed using a Bruker X8 APEX II CCD diffractometer with kappa geometry and Mo−Kα radiation (λ = 0.71073 Å). Data integration was performed using the SAINT software suite. Data processing, including absorption corrections from equivalent reflections, was performed using SADABS.[10] Direct methods (SHELXS97) solutions successfully located the W atoms, and successive Fourier syntheses (SHELXL97) revealed the remaining atoms.[11] Refinements were full-matrix least-squares against $|F|^2$ using all data. Cations and waters of hydration were modeled with varying degrees of occupancy, a common situation in polyoxotungstate crystallography. In the final refinements, all nondisordered heavy atoms (W, K, P, Co, Mn, Ni, V) were refined anisotropically, while the O atoms and some disordered counter cations were refined isotropically. Crystallographic data are shown in Table 1.

UV−Visible Spectroscopy. Pure water was used throughout, and it was obtained by passing through a RiOs 8 unit followed by a Millipore-Q Academic purification set. All reagents were of high-purity grade and were used as purchased without further purification. The UV−visible spectra were recorded on a Perkin-Elmer Lambda 19 spectrophotometer on 1 × 10^{-5} M solutions of **1**. Matched 1.000 cm optical path quartz cuvets were used. The following media proved useful for the present study: 0.5 M H_2SO_4 pH = 0.33; 1 M LiCl/HCl, pH = 3; 1 M CH_3CO_2Li/CH_3CO_2H, pH = 5; and 0.5 M Li_2SO4 + 0.1 M TRIS + H_2SO_4, pH = 7.

Electrochemical Experiments. The solutions were deaerated thoroughly for at least 30 min with pure argon and kept under a positive pressure of this gas during the experiments. The source, mounting, and polishing of the glassy carbon (GC, Tokai, Japan) electrodes has been described.[12] The glassy carbon samples had a diameter of 3 mm. The electrochemical setup was an EG & G 273 A driven by a PC with the M270 software. Potentials are quoted against a saturated calomel electrode (SCE). The counter electrode was a platinum gauze of large surface area. All experiments were performed at room temperature.

Magnetic Susceptibility, Magnetization, and EPR Measurements. Direct current (dc) magnetic susceptibility measurements on powder samples of **KLi-1**, **KLi-2**, and **KLi-3** were carried out using a Quantum Design MPMS-XL SQUID magnetometer over the temperature range 1.8−250 K and at 0.1 T applied magnetic field. Magnetization as a function of applied magnetic field was measured at 1.8 K in the range 0−7 T using the same SQUID magnetometer. The experimental data were fit using the usual nonlinear least-squares method of the software "Origin", and the reported errors were obtained from the statistical weighting of the experimental data in the fit. Multi-frequency (34−413 GHz) EPR spectra were obtained on the above powder samples in the temperature range 5−295 K. While the Q-band ($\nu \sim$ 34 GHz) spectra were recorded using a Bruker Elexsys-500 spectrometer, those at higher frequencies were obtained using a custom-built variable frequency EPR spectrometer equipped with a 15 T superconducting magnet at the National High Magnetic Field Laboratory in Tallahassee.[13] The spectra were simulated using an in-house program called "Spin" written by Dr. Andrzej Ozarowski. The errors reported are from a visual comparison of the simulations with the experimental spectra for different sets of simulations parameters.

(10) Sheldrick, G. M. *SADABS*; University of Göttingen: Göttingen, Germany, 1996.
(11) Sheldrick, G. M. *SHELX-97, Program for Solution of Crystal Structures*; University of Göttingen: Göttingen, Germany, 1997.
(12) Keita, B.; Nadjo, L. *J. Electroanal. Chem.* **1988**, *243*, 87.
(13) (a) Cage, B.; Hassan, A. K.; Pardi, L.; Krzystek, J.; Brunel, L. C.; Dalal, N. S. *J. Magn. Reson.* **1997**, *124*, 495. (b) Hassan, A. K.; Pardi, L. A.; Krzystek, J.; Sienkiewicz, A.; Goy, P.; Rohrer, M.; Brunel, L. C. *J. Magn. Reson.* **2000**, *142*, 300.

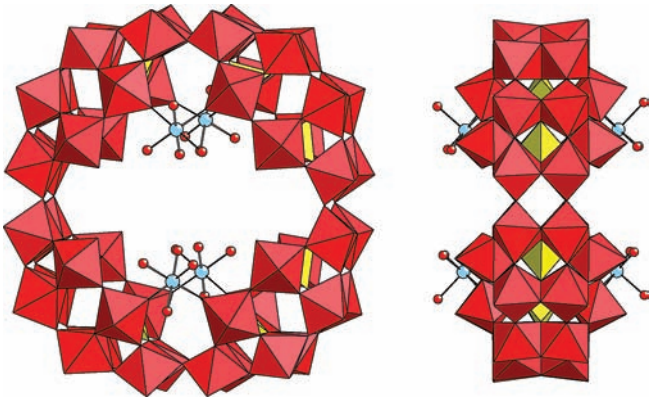

Figure 1. Top (left) and side (right) view of $[Co_4(H_2O)_{16}P_8W_{48}O_{184}]^{32-}$ (**1**). Color code: WO_6 red, PO_4 yellow, Co pale-blue, O red.

Results and Discussion

Synthesis and Structure. The tetra-cobalt(II) containing 48-tungsto-8-phosphate $[Co_4(H_2O)_{16}P_8W_{48}O_{184}]^{32-}$ (**1**) was prepared by reaction of Co^{2+} ions with $\mathbf{P_8W_{48}}$ in a 25:1 molar ratio in pH 5.3 lithium acetate buffer at 80 °C. The solid state structure of **1** (see Figure 1) reveals four Co^{2+} ions coordinated to the inner rim of the cyclic tungstophosphate precursor. The detailed binding sites are as expected the oxygens of the terminal W−O bonds pointing toward the center of the polyanion. Interestingly, only half of these sites are occupied (8 out of 16) by the four Co^{2+} ions, which are each coordinated in a *cis* fashion to two O(W) atoms from two adjacent $\{P_2W_{12}\}$ subunits with an average bond length of 2.05(2) Å. The remaining four terminal coordination sites are occupied by water ligands with an average bond length of 2.10(2) Å. The four cobalt centers are coplanar, and their plane is orthogonal to the main plane of the $\mathbf{P_8W_{48}}$ ligand host, resulting in D_{2h} point group symmetry for **1**. Polyanion **1** is the second example of a cobalt(II)-containing $\mathbf{P_8W_{48}}$. Cronin's group reported recently the synthesis and solid state structure of two hexa-cobalt(II)-containing $\mathbf{P_8W_{48}}$ derivatives, with four external cobalt(II) ions linking adjacent polyanions resulting in chains and networks.[14] Their polyanions have a similar structure to ours, but two additional cobalt(II) ions are disordered over four equivalent positions within the $\mathbf{P_8W_{48}}$ ring. The coordination in our polyanion **1** results in a slight "oval" distortion of the $\mathbf{P_8W_{48}}$ assembly, as reflected by a difference of ca. 1.6 Å between the "length" (18.5 Å polyanion diameter of opposite W centers in the plane of the cobalt(II) centers) and the "width" (16.9 Å polyanion diameter of opposite W centers perpendicular to the previous plane). This kind of distortion was observed as well in our previously reported organometallic $\mathbf{P_8W_{48}}$ derivative $[\{K(H_2O)\}_3\{Ru(p\text{-cymene})(H_2O)\}_4P_8W_{49}O_{186}(H_2O)_2]^{27-}$.[7b] In addition to the four cobalt(II) centers coordinated to the inner rim of $\mathbf{P_8W_{48}}$, we also found two outer Co^{2+} ions in **1** bridging neighboring polyanions and forming a chain in the solid-state (see Supporting Information Figure S1). Polyanion **1** crystallizes as a mixed potassium−lithium salt $K_{12}Li_{16}Co_2[Co_4(H_2O)_{16}P_8W_{48}O_{184}]\cdot 60H_2O$ (**KLi-1**) in the triclinic space group $P\bar{1}$.

(14) Mitchell, S. G.; Gabb, D.; Ritchie, C.; Hazel, N.; Long, D. L.; Cronin, L. *CrystEngComm* **2009**, *11*, 36.

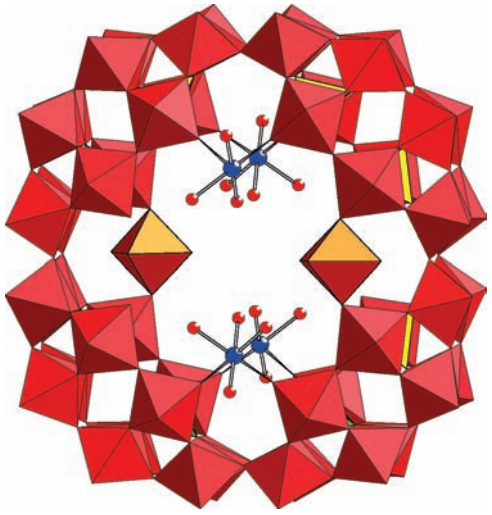

Figure 2. Top view of $[M_4(H_2O)_{16}(P_8W_{48}O_{184})(WO_2(H_2O)_2)_2]^{28-}$ (M = Mn **2**, Ni **3**). The color code is the same as in Figure 1 except Mn/Ni is blue. The two extra WO_6 octahedra are shown in orange. See text for details.

The precise number of potassium and lithium counter cations was verified by elemental analysis.

When performing the above reaction under similar conditions for Mn^{2+} instead of Co^{2+}, and by adding a few drops of H_2O_2 during the synthesis, we obtained the novel polyanion $[Mn_4(H_2O)_{16}(P_8W_{48}O_{184})(WO_2(H_2O)_2)_2]^{28-}$ (**2**); see Figure 2. Such an apparent small change in the synthetic procedure has a dramatic effect on the resulting polyanion structure. In addition to the four Mn^{2+} ions, which are linked to the $\mathbf{P_8W_{48}}$ ligand in an identical fashion as the Co^{2+} ions in **1**, polyanion **2** exhibits two extra WO_6 octahedra disordered over the four identical positions perpendicular to the plane of the Mn^{2+} ions. Therefore, we have discovered the novel $\{P_8W_{50}\}$ tungstophosphate host. When performing this reaction with Ni^{2+} instead of Mn^{2+} we obtained the isostructural polyanion $[Ni_4(H_2O)_{16}(P_8W_{48}O_{184})(WO_2(H_2O)_2)_2]^{28-}$ (**3**). Both polyanions **2** and **3** have point group symmetry C_{2h}. The "extra" tungsten centers in **2** and **3** are coordinated to the exact same types of oxygens of the $\mathbf{P_8W_{48}}$ wheel as the Mn^{2+}/Ni^{2+} ions, but in a *trans* fashion. The four equatorial, terminal ligands are a *cis*-oxo and a *cis*-aqua pair, the former pointing toward the center of the polyanion. This is an analogous situation as for the twofold disordered, extra WO_6 octahedron of the $\{P_8W_{49}\}$ host in our $\{K(H_2O)\}_3\{Ru(p\text{-cymene})(H_2O)\}_4P_8W_{49}O_{186}(H_2O)_2]^{27-}$.[7b] The above-mentioned distortion of the $\mathbf{P_8W_{48}}$ wheel in **1** is also observed for **2** and **3**, but to a much lesser degree (18.3 vs 17.1 Å perpendicular polyanion diameters), most likely due to the coordination of the extra tungsten atoms. Compared to polyanion **1**, the average M−O(W) distance for the Mn^{2+} centers in **2** is 2.13(2) Å and 2.02(2) Å for the Ni^{2+} centers in **3**. The respective average M−O(aqua) bonds are 2.20(2) and 2.06(2) Å for Mn^{2+} in **2** and Ni^{2+} in **3**, respectively. As mentioned above, polyanions **2** and **3** do not form without addition of hydrogen peroxide during the synthesis, which may be regarded as an "activation" agent for $\mathbf{P_8W_{48}}$ allowing for coordination of manganese(II) or nickel(II) accompanied by grafting of 2 equiv of tungsten. The additional tungsten atoms are believed to originate from

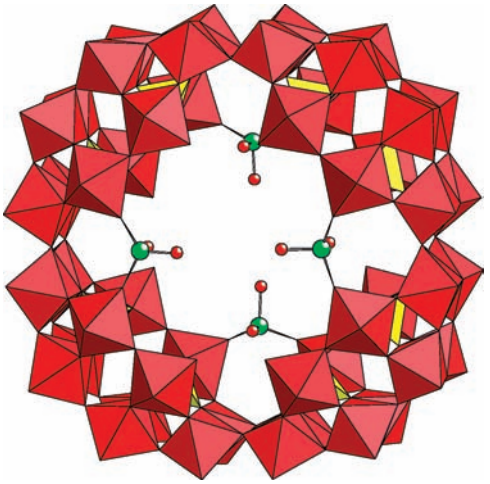

Figure 3. Top view of $[(VO_2)_4(P_8W_{48}O_{184})]^{36-}$ (**4**). The color code is the same as in Figure 1 except V is green.

decomposition of a minute amount of $\mathbf{P_8W_{48}}$. It could well be that hydrogen peroxide initiates and/or assists such decomposition and, at the same time, activates the $\mathbf{P_8W_{48}}$ wheel for condensation of extra tungsten units. However, when performing the synthesis of polyanion **1** in the presence of H_2O_2, we did not observe condensation of extra W ions. Polyanions **2** and **3** crystallize as mixed potassium−lithium salts, $K_{12}Li_{10}Mn_3[Mn_4(H_2O)_{16}(P_8W_{48}O_{184})(WO_2(H_2O)_2)_2]\cdot 67H_2O$ (**KLi-2**) and $K_{14}Li_8Ni_3[Ni_4(H_2O)_{16}(P_8W_{48}O_{184})(WO_2(H_2O)_2)_2]\cdot 44H_2O$ (**KLi-3**), respectively, in the triclinic space group $P\bar{1}$. The presence of three Mn^{2+} counter cations in **KLi-2** and three Ni^{2+} counter cations in **KLi-3** were identified by elemental analysis, but not by single-crystal XRD most likely due to disorder.

We were also able to prepare the tetra-vanadate derivative $[(VO_2)_4(P_8W_{48}O_{184})]^{36-}$ (**4**, see Figure 3) by using the same synthetic procedure as for **1** but replacing Co^{2+} by VO^{2+}. The vanadium centers in **4** are clearly in the +5 oxidation state, as indicated by bond valence sum (4.83)[15] and chemical composition. It appears that V^{4+} is oxidized to V^{5+} during the course of the reaction, most likely due to air oxidation. Polyanion **4** is also structurally related to **1**, except that four tetrahedral VO_4 groups (average V−O distances: V−O(W) 1.65(2) Å and V−O(terminal) 1.84(1) Å) are grafted to the inner rim of $\mathbf{P_8W_{48}}$ instead of the octahedrally coordinated Co^{2+} centers. In addition, the respective positions of the Co^{2+} and V^{5+} centers are not the same. Whereas all four Co^{2+} ions are coplanar, this is not the case for the vanadate units. The latter are located at four donor positions inside the $\mathbf{P_8W_{48}}$ wheel which are mutually oriented tetrahedrally to each other, or in other words, which alternate up−down with respect to the plane of the eight phosphorus atoms in **4**. Opposite of each vanadium ion, with respect to this plane, is a potassium countercation. In the solid state, these four positions show a 50% vanadium/potassium disorder over a total of 8 positions. Such symmetrical disorder is reflected by the tetragonal space group $P4/m$ of the polyanion salt $K_{20}Li_{16}[(VO_2)_4(P_8W_{48}O_{184})]\cdot 48H_2O$ (**KLi-4**).

(15) Brown, I. D.; Altermatt, D. *Acta Crystallogr.* **1985**, *B41*, 244.

We also performed multinuclear NMR studies on **KLi-4** redissolved in water. In ^{31}P NMR, we observed a singlet at −8.1 ppm and ^{51}V NMR showed a singlet at −559.4 ppm, both fully supportive of the proposed structure for **4**.

In **1**−**3** the incorporated 3d transition metal ions are isolated from each other, which is in sharp contrast to our Cu_{20} and Fe_{16} derivatives $[Cu_{20}X(OH)_{24}(H_2O)_{12}(P_8W_{48}O_{184})]^{25-}$ (X = Cl, Br, I) and $[Fe_{16}(OH)_{28}(H_2O)_4P_8W_{48}O_{184}]^{20-}$, respectively, which both exhibit aesthetic multinuclear coordination complex assemblies with μ_2-hydroxo/aqua bridged metal ions. It is not evident why similar multi-cobalt(II)/manganese(II)/nickel(II) clusters could not be assembled inside the $\mathbf{P_8W_{48}}$ template.

Electrochemistry

It was anticipated from our previous work on analogous POMs that pH variations might be encountered upon dissolution of increasing amounts of the present polyanions in solution.[16−19] This trend was confirmed experimentally for **1** (see Supporting Information Figure S2). As a consequence, media with a high acidity as pH = 0.33 and buffers with a large capacity such as 1 M $CH_3COOLi + CH_3COOH$ (pH 5) were selected for subsequent studies of the polyanions.

In the following, **1** is selected as a representative polyanion for which detailed electrochemical characterization will be provided. The potential domain is divided in a positive and a negative one (vs SCE), for a sequential description of the observed phenomena, thus allowing to separate the possible features specifically related to the presence of the Co^{2+} ions. In the pH = 0.33 medium and in the negative potential domain, the cyclic voltammogram (CV) of **1** shows five W-waves as shown in Figure 4A. The first four are chemically reversible and the last one is irreversible and close to the electrolyte discharge limit. The first W-wave of **1** is diffusion-controlled as indicated by the good linearity of its peak current variation as a function of the square root of the scan rate (inset in Figure 4A). The average difference between the anodic and the cathodic peak potentials is 70 mV for scan rates varying from 2 to 100 mV s^{-1}.

It is worth noting that the whole pattern in Figure 4A resembles qualitatively that associated with the $\mathbf{P_8W_{48}}$ precursor in the same electrolyte. Therefore, analogies and differences between the electrochemical behaviors of **1** and its precursor $\mathbf{P_8W_{48}}$ are briefly highlighted in the following. To illustrate this behavior, Figure 4B shows the CV of **1** restricted to its first two W-waves in superposition with the corresponding waves of $\mathbf{P_8W_{48}}$. As the main difference, the first two waves of **1** appear to be better separated and are located at slightly more negative potentials than the corresponding ones of $\mathbf{P_8W_{48}}$. Thus, an electrochemical−chemical−electrochemical (ECE) or an electrochemical−electrochemical−chemical (EEC) type process is favored in the case of $\mathbf{P_8W_{48}}$. It must be concluded that the reduced forms of **1** are less basic than the corresponding forms of

(16) Keita, B.; Lu, Y. W.; Nadjo, L.; Contant, R. *Electrochem. Commun.* **2000**, *2*, 720.
(17) Keita, B.; Lu, Y. W.; Nadjo, L.; Contant, R *Eur. J. Inorg. Chem.* **2000**, 2463.
(18) Bassil, B. S.; Nellutla, S.; Kortz, U.; Stowe, A. C.; van Tol, J.; Dalal, N. S.; Keita, B.; Nadjo, L. *Inorg. Chem.* **2005**, *44*, 2659.
(19) Keita, B.; de Oliveira, P.; Nadjo, L.; Kortz, U. *Chem.—Eur. J.* **2007**, *13*, 5480.

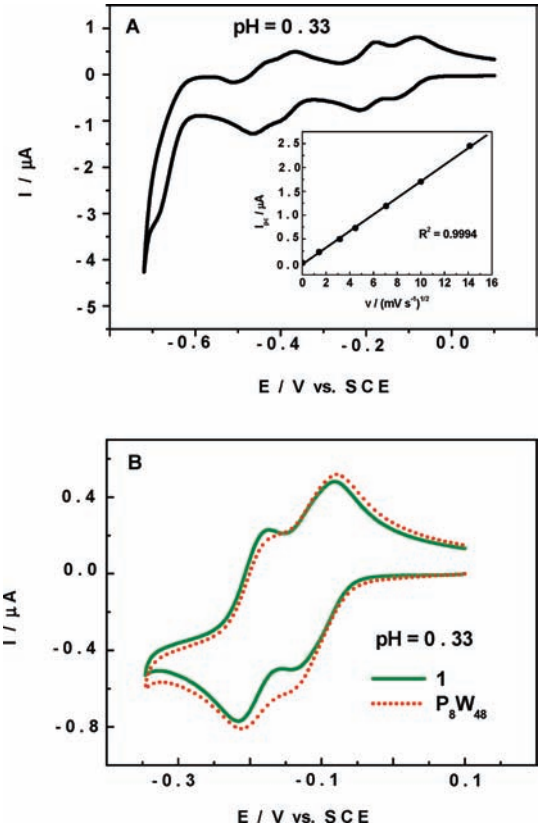

Figure 4. Cyclic voltammetric (CV) studies of 4×10^{-5} M polyanion **1** in pH 0.33 (0.5 M H_2SO_4) medium. The working electrode was glassy carbon and the reference electrode was SCE. The scan rate was 10 mV s^{-1}. (A) Main voltammetric pattern associated with the reduction of W^{VI}-centers of **1** in a pH 0.33 medium. (inset) Variation of the peak current intensity for the first W^{VI}-wave of **1** as a function of the square root of the potential scan rate. (B) Superposition of the CV of **1**, restricted to its first two W^{VI}-waves (green curve) and the corresponding waves of the precursor $\mathbf{P_8W_{48}}$ (red dotted curve) in a pH 0.33 medium.

$\mathbf{P_8W_{48}}$.[20] The same trend also holds for the two subsequent waves (not shown). For an easy comparison with $\mathbf{P_8W_{48}}$, controlled potential coulometry was performed at −0.290 V vs SCE, a potential allowing for simultaneous electrolysis on the first two waves in Figure 4B. The result indicates the consumption of 8.01 ± 0.05 electrons per molecule of **1**, in full agreement with the value obtained for coulometry on $\mathbf{P_8W_{48}}$ at identical experimental conditions.[16] After exhaustive electrolysis of **1** at −0.290 V vs SCE, the reduced solution could be reoxidized quantitatively at +0.1 V vs SCE to its initial state, thus proving the stability of both the oxidized and reduced forms of this polyanion in the pH = 0.33 medium. Figure 5 shows a comparison of the CVs of **1** at pH = 0.33 and pH = 5. Strikingly, the system of four separate waves observed at pH = 0.33 is replaced by a system of two waves. The peak current of the first wave obtained at pH = 5 remains roughly equal to the combined peak current intensities of the first two waves measured at pH = 0.33. The same observation is valid for the second wave observed at pH = 5, and the combined peak current intensities of the third and the fourth waves of **1** at pH = 0.33. Such merging of waves with increasing pH is unusual in POM electrochemistry but

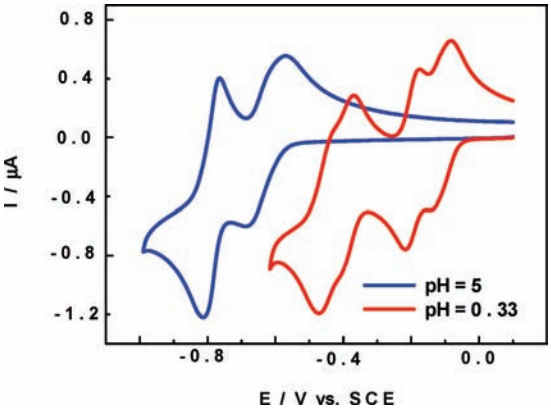

Figure 5. Evolution of the CV of 4×10^{-5} M polyanion **1** in pH 0.33 (0.5 M H_2SO_4) (red curve) and pH 5 (1 M CH_3CO_2Li/CH_3CO_2H) (blue curve) media. The working electrode was glassy carbon and the reference electrode was SCE. The scan rate was 10 mV s^{-1}.

is not unprecedented and corresponds to an inversion of acidities among some of the reduced species of the relevant POM.[16,18,21] Analogous observations were made with $\mathbf{P_8W_{48}}$,[16] 18-molybdo-2-phosphate,[21] and 18-molybdo-2-arsenate.[22] For example, it was demonstrated that the tenth acidity of the four-electron reduced species of 18-molybdo-2-arsenate is weaker than the tenth acidity of the six electron-reduced compound.[22] The inversion of acidities, demonstrated clearly in this example, might constitute a general rationale for such observations.

To detect the Co^{2+} centers of **1**, the potential was first scanned toward the positive direction. Even in successful examples, this challenging issue generally necessitates the appropriate choice of supporting electrolyte and/or some treatment of the electrode surface. In the present case, such observation of Co^{2+} ions within polyanion **1** was successful at pH = 5, (Supporting Information Figure S3) with a chemically irreversible two-step anodic pattern with peaks located roughly at +0.975 V, and +1.200 V vs SCE. In any case, the observation of some electroactivity is rewarding in itself, because, it is known that Co^{2+} detection in multicobalt POMs is usually unsuccessful, except for a few recent examples.[18,23,24] Beforehand, only monosubstituted POMs and $[Co^{II}W_{12}O_{40}]^{6-}$ were shown to display an electroactive Co center.[25]

The electrochemical behaviors of polyanions **2** and **4** were also studied by cyclic voltammetry. In short, in analogy to the cobalt(II) containing **1**, also the Mn^{2+} and V^{5+} ions in **2** and **4**, respectively, modify the acid−base properties of the W skeleton. In addition to Figure 4B, which compares the CVs of **1** and $\mathbf{P_8W_{48}}$, Supporting Information Figure S4 shows the CVs of **2** and **4**. These influences due to the substituting 3d metal ions are reflected both in the potential locations and separations of the W-waves. Even though small, these parameters allow for a qualitative evaluation of the relative basicity of the reduced polyanions, resulting in the following

(20) Keita, B.; Mbomekalle, I. M.; Lu, Y. W.; Nadjo, L.; Berthet, P.; Anderson, T. M.; Hill, C. L. *Eur. J. Inorg. Chem.* **2004**, *17*, 3462.

(21) Papaconstantinou, E.; Pope, M. T. *Inorg. Chem.* **1967**, *6*, 1152.

(22) Contant, R.; Fruchart, J. M. *Revue Chim. Minérale* **1974**, *11*, 123.

(23) Lisnard, L.; Mialane, P.; Dolbecq, A.; Marrot, J.; Clemente-Juan, J. M.; Coronado, E.; Keita, B.; de Oliveira, P.; Nadjo, L.; Sécheresse, F. *Chem.—Eur. J.* **2007**, *13*, 3527.

(24) Bassil, B. S.; Kortz, U.; Tigan, A. S.; Clemente-Juan, J. M.; Keita, B.; de Oliveira, P.; Nadjo, L. *Inorg. Chem.* **2005**, *44*, 9360.

(25) Keita, B.; Lu, Y. W.; Nadjo, L.; Contant, R.; Abbessi, M.; Canny, J.; Richet, M. *J. Electroanal. Chem.* **1999**, *477*, 146.

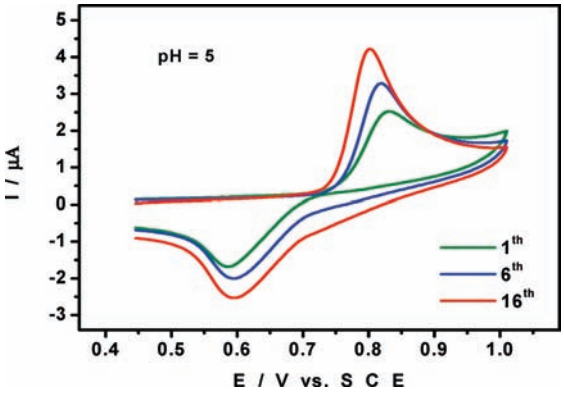

Figure 6. Evolution of the CV of 4×10^{-5} M polyanion **2** in a pH 5 (1 M CH_3CO_2Li/CH_3CO_2H) medium showing the redox activity of the Mn^{2+} centers. The 1st, 6th, and 16th CVs are shown. The working electrode was glassy carbon and the reference electrode was SCE. The scan rate was 10 mV s^{-1}.

sequence: **2** > $\mathbf{P_8W_{48}}$ > **1** > **4**. Specific information can be obtained from a study of the heteroatoms themselves within the polyanions. For the Mn and V derivatives **2** and **4** we focused mainly on the selected media in which the behaviors are best behaved.

As usual, the detection of Mn centers within substituted POMs is a challenge. In the present case, the Mn^{2+} ions associated with polyanion **2** are not voltammetrically detected at pH = 0. Gradual improvement is obtained as the pH of the electrolyte rises, with the best detection observed at pH = 5. Figure 6 summarizes the behavior of the Mn centers. The CV constitutes a single quasi-reversible wave with a relatively sharp oxidation peak and a broad reduction wave upon potential reversal. The oxidation peak potential of the first CV is located at +0.830 V vs SCE. With each following potential cycle, the oxidation peak current intensity keeps increasing while the corresponding peak potential moves in the negative direction. Such behavior indicates gradual deposition of the electroactive material on the electrode, with a progressive activation of the electrode surface. A similar film deposition behavior upon oxidation of a Mn^{2+} center was encountered previously in the electrochemical study of $[(1),2,3\text{-}PMo_2W_{15}O_{61}]^{10-}$ substituted by a Mn^{2+} ion[25] and in the electrodeposition of electroactive metal oxide films from POMs.[26] Such deposit formation prevents determination of the number of electrons involved in the oxidation process and, correspondingly, counting of the number of electroactive Mn centers in the compound. Future work will focus on the composition of this film and on its properties.

The V centers in polyanion **4** display electrochemical behaviors (Supporting Information Figure S5) that depend on the scan rate. For example, in a pH = 0.33 medium, the reversibility of the V^V/V^{IV} redox couple is poor at a slow scan rate. A good reoxidation can be recovered by increasing the scan rate.

Magnetism

dc Magnetic Susceptibility and Magnetization. In **1**−**3** the four M^{2+} (M = Co, Mn, Ni) ions which are coordinated on the inside of the $\mathbf{P_8W_{48}}$ wheel ("core" ions) are rather far from each other ($M_{inner}\cdots M_{inner} \sim 8-9$ Å) suggesting that, magnetically, they act as independent paramagnetic ions. Further, the crystal structures of **1**−**3** together with the respective elemental analyses suggest varying numbers of M^{2+} ions in external positions (e.g., four Co^{2+} ions linking three adjacent $\mathbf{P_8W_{48}}$ wheels), referred here as "outer" ions. Therefore, the total number, n, of M^{2+} ions per formula unit of **KLi-1**, **KLi-2**, and **KLi-3**, is 6, 7, and 7, respectively. The magnetic data of these compounds was analyzed fixing n at the respective value.

The molar magnetization M and magnetic susceptibility χ of a paramagnetic ion are given as[27,28b]

$$M = NkT\left(\frac{\partial \ln Z}{\partial H}\right) \tag{1}$$

$$\chi = N\left[\frac{\sum_i \left[\left(\frac{(E_i^{(1)})^2}{kT}\right) - 2E_i^{(2)}\right]\exp(-E_i^{(0)}/kT)}{\sum_i \exp(-E_i^{(0)}/kT)}\right] \tag{2}$$

Here, Z is the partition function written as $\sum_i \exp(-E_i/kT)$, N is Avogadro's number, k is the Boltzmann constant, and T is the temperature. $E_i^{(0)}$ is the energy of the i^{th} level in zero field, $E_i^{(1)}$ and $E_i^{(2)}$ are, respectively, the first and second order Zeeman energies. Finally, we would like to note that eq 2 is applicable[27] only in the range where M is linear in H and the summation runs over all the energy levels.

Analysis of M vs H and χ vs T of **KLi-1**, **KLi-2**, and **KLi-3** has been done under the following assumptions: (i) the spin Hamiltonian parameters are same for both types of M^{2+} sites since the coordination environment of the "core" and "outer" M^{2+} ions is similar. (ii) The site symmetry around each M^{2+} ion is considered as axial, which implies that the rhombic zero-field splitting parameter $E = 0$. Also, other higher-order terms of the spin Hamiltonian are neglected. (iii) Only one g-value (g_{iso}) was used, not only because the data was collected on powder samples, but also to reduce the number of fit parameters. We would like to note that the perpendicular (i.e., $H \perp z$-axis) energy equations published in the literature[27] for $|D| \gg g_x\mu_B H_x$ have been used to calculate $M_\perp$ and $\chi_\perp$ in eqs 1 and 2, respectively. The spin Hamiltonian corresponding to assumption (ii) can be written as[27,28]

$$\hat{\mathbf{H}} = g_u\mu_B\hat{\mathbf{S}}_u H_u + D[\hat{\mathbf{S}}_z^2 - S(S+1)/3] \tag{3}$$

where, the subscript "u" denotes the direction of the applied field H, μ_B is the Bohr magneton, g_u and $\hat{\mathbf{S}}_u$ are, respectively, the g-value and spin operator component along u, S the spin value, and D the axial zero-field splitting parameter. The S values of Co^{2+}, Mn^{2+}, and Ni^{2+} in **KLi-1**, **KLi-2**, and **KLi-3**, respectively, are 3/2, 5/2, and 1.

(26) Keita, B.; Abdeljalil, E.; Girard, F.; Gerschwiler, S.; Nadjo, L.; Contant, R.; Haut, C. *J. Solid State Electrochem.* **1999**, *3*, 446.

(27) (a) Kahn, O. *Molecular Magnetism*; VCH: New York, 1993. (b) Carlin, R. L. *Magnetochemistry*; Springer-Verlag: New York, 1986.

(28) (a) Abragam, A.; Bleaney, B. *Electron Paramagnetic Resonance of Transition Ions*; Dover Publications: New York, 1970. (b) Griffith, J. S. *The Theory of Transition Metal ions*; Cambridge University Press: Cambridge, 1961.

Scheme 1. Splitting of the Co^{2+} Free-Ion ^4F Ground State under the Influence of (a) Crystal Field, (b) Tetragonal Distortion, and (c) Spin-Orbit Coupling

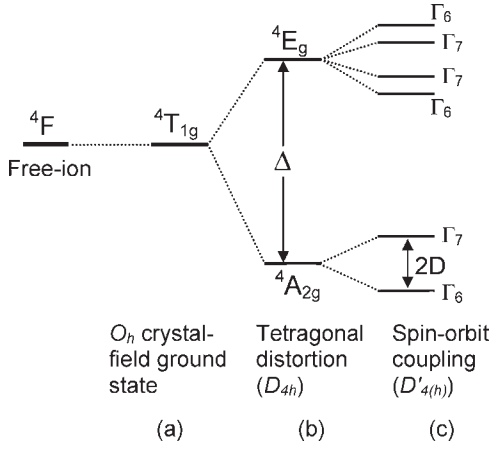

$K_{12}Li_{16}Co_2[Co_4(H_2O)_{16}P_8W_{48}O_{184}]\cdot 60H_2O$ (KLi-1). The near axial environment of the Co^{2+} ions in **KLi-1** splits the $^4T_{1g}$ ground state into an orbital singlet ($^4A_{2g}$) and an orbital doublet (^4E_g), which are then split into Kramers doublets by spin−orbit coupling (cf. Scheme 1). When the separation, Δ, between $^4A_{2g}$ and ^4E_g is large, the magnetic properties can be interpreted considering only the two lowest Kramers doublets Γ_6 ($M_S = \pm 1/2$) and Γ_7 ($M_S = \pm 3/2$) arising from $^4A_{2g}$.[27,28] The effect of the orbital momentum, although not considered explicitly, has been incorporated into the *D*- and *g*-values of eq 3 and therefore the spin remains as $S = 3/2$. Figure 7 shows the experimental magnetic susceptibility of **KLi-1** plotted as μ_{eff} vs T, where μ_{eff} is related[27] to $\chi(T)$ as shown in eq 4. Here, $\chi(T)$ is given by eq 2.

$$\mu_{eff} = \sqrt{\frac{3kT}{N}\chi(T)} \qquad (4)$$

The room temperature $\mu_{eff} \sim 5.7\mu_B$ is consistent with a high-spin Co^{2+} in an octahedral environment.[27−35] As can be seen from the figure, the data can be reasonably well described by eq 4 with the parameters listed in Table 2, where θ is the Curie−Weiss constant which accounts for interactions between the M^{2+} ions. Figure 8a shows the field dependence of magnetization for **KLi-1** obtained at 1.8 K. Our attempts to reproduce the data using eq 1 are reasonably successful with values listed in Table 2. The discrepancy could be due to ignorance of rhombic zero-field splitting parameter *E* and/or interactions between the Co^{2+} ions.

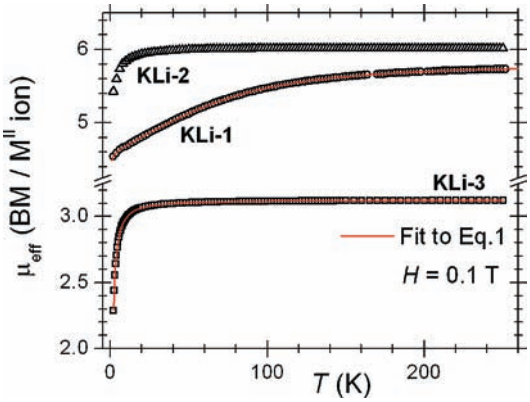

Figure 7. Temperature dependence of μ_{eff} per magnetic ion for **KLi-1**, **KLi-2**, and **KLi-3**. The solid lines represent the theoretical fits. See text for details.

However, the *g*- and *D*-values are consistent between the two types of measurements and in line with the literature values[27−35] for axially distorted Co^{2+} ions.

$K_{12}Li_{10}Mn_3[Mn_4(H_2O)_{16}(P_8W_{48}O_{184})(WO_2(H_2O)_2)_2]\cdot 67H_2O$ (KLi-2). Figures 7 and 8b, respectively, display the μ_{eff} vs T and M vs H for **KLi-2**. The observed room temperature value of $\sim 6\mu_B$ in Figure 7 and the high-field saturation value of $\sim 5\mu_B$ in Figure 8b are consistent with the spin-only nature of a high-spin Mn^{2+} ion.[27,29,36−39] Analysis of μ_{eff} vs T for **KLi-2** using eq 4 yields a $|D|$ value approximately five times larger than that obtained from EPR (vide infra). Since EPR is always more accurate than susceptibility for the determination of *D*, we trust the former more and therefore the temperature dependence of μ_{eff} will not be discussed further. As can be seen from Figure 8b, the overall M vs H profile for **KLi-2** not only echoes with that of the Brillouin function expected[27] for a $S = 5/2$ with $g = 2$ but also exhibits relatively small deviation in the field range ~0.8−4.5 T. We therefore deduce that the magnitude of *D* should be relatively small, in agreement with EPR (vide infra). In fact, when we simulated the data (data not shown) using eq 1 for $H \parallel z$-axis, we observed a $|D| \sim 0.4$ K. Since $D < g_x\mu_B H_x$, an in-depth analysis of the field dependence of the magnetization for **KLi-2** would require a numerical evaluation of eq 1 rather than the analytical approach adapted for **KLi-1** and therefore is beyond our computational capabilities at the moment.

$K_{14}Li_8Ni_3[Ni_4(H_2O)_{16}(P_8W_{48}O_{184})(WO_2(H_2O)_2)_2]\cdot 44H_2O$ (KLi-3). While Figure 7 displays the μ_{eff} vs T for **KLi-3**, Figure 8c shows its M vs H behavior. The experimental room temperature value of $\sim 3.1\mu_B$ in Figure 7, and the high-field magnetization value of $\sim 2.3\mu_B$ in Figure 8c are consistent with spin-only values of octahedral Ni^{2+} ions.[27,35,39−41] As can

(29) Krzystek, J.; Ozarowski, A.; Telser, J. *Coord. Chem. Rev.* **2006**, *250*, 2308.
(30) Lloret, F.; Julve, M.; Cano, J.; Ruiz-García, R.; Pardo, E. *Inorg. Chim. Acta* **2008**, *361*, 3432.
(31) Ostrovsky, S.; Tomkowicz, Z.; Haase, W. *Coord. Chem. Rev.* **2009**, *253*, 2363.
(32) Lohr, L. L.; Miller, J. C.; Sharp, R. R. *J. Chem. Phys.* **1999**, *111*, 10148.
(33) Waldmann, O.; Hassmann, J.; Müller, P.; Hanan, G. S.; Volkmer, D.; Schubert, U. S.; Lehn, J.-M. *Phys. Rev. Lett.* **1997**, *78*, 3390.
(34) Figgis, B. N.; Gerloch, M.; Lewis, J.; Mabbs, F. E.; Webb, G. A. *J. Chem. Soc. A* **1968**, 2086.
(35) (a) Juric, M.; Peric, B.; Brnicevic, N.; Planinic, P.; Pajic, D.; Zadro, K.; Giester, G.; Kaitner, B. *Dalton Trans.* **2008**, 742. (b) Becker, R.; Prester, M.; Berger, H.; Lin, P. H.; Johnsson, M.; Drobac, D.; Zivkovic, I. *J. Solid State Chem.* **2007**, *180*, 1051.
(36) Jain, V. K.; Lehmann, G. *Phys. Stat. Sol. B* **1990**, *159*, 495.
(37) Wang, M.; Ma, C.; Wen, H.; Chen, C. *Dalton Trans.* **2009**, 994.
(38) Shit, S.; Chakraborty, J.; Samanta, B.; Slawin, A. M. Z.; Gramlich, V.; Mitra, S. *Struct. Chem.* **2009**, *20*, 633.
(39) Misra, S. K.; Andronenko, S. I.; Earle, K. A.; Freed, J. H. *Appl. Magn. Reson.* **2001**, *21*, 549.
(40) (a) Lin, J.-D.; Jia, C.-C.; Li, Z.-H.; Du, S.-W. *Inorg. Chem. Commun.* **2009**, *12*, 558. (b) Zhao, Y.-R.; Kuang, X.-Y.; Lu, C.; Duan, M.-L.; Zheng, B.-B. *Mol. Phys.* **2009**, *107*, 133. (c) Cernak, J.; Paharova, J.; Kuchar, J.; Zak, Z.; Taraba, J.; Kajnakova, M.; Orendac, M. *J. Coord. Chem.* **2008**, *61*, 3357.
(41) (a) Maslejova, A.; Ivanikova, R.; Svoboda, I.; Papankova, B.; Dlhan, L.; Miklos, D.; Fuess, H.; Boca, R. *Polyhedron* **2006**, *25*, 1823. (b) Yang, Z. Y.; Hao, Y.; Rudowicz, C.; Yeung, Y. Y. *J. Phys.: Condens. Matter* **2004**, *16*, 3481. (c) Waldmann, O.; Hassmann, J.; Muller., P.; Volkmer, D.; Schubert, U. S.; Lehn, J. M. *Phys. Rev. B.* **1998**, *58*, 3277.

Table 2. Magnetic Parameters Obtained from the Fit of Magnetization and Magnetic Susceptibility to Equations 1 and 2

		magnetic susceptibility			magnetization	
	n	g_{iso}	$\|D/k\|$ (K)	θ (K)	g_{iso}	$\|D/k\|$ (K)
KLi-1	6	2.99 ± 0.15	128 ± 6	-0.05 ± 0.003	2.70 ± 0.15	110 ± 5^a
KLi-2	7					
KLi-3	7	2.21 ± 0.11	-7.5 ± 0.5^a	-0.66 ± 0.03		

[a] Sign of D is assigned based on the R^2 value from the nonlinear least-squares fitting.

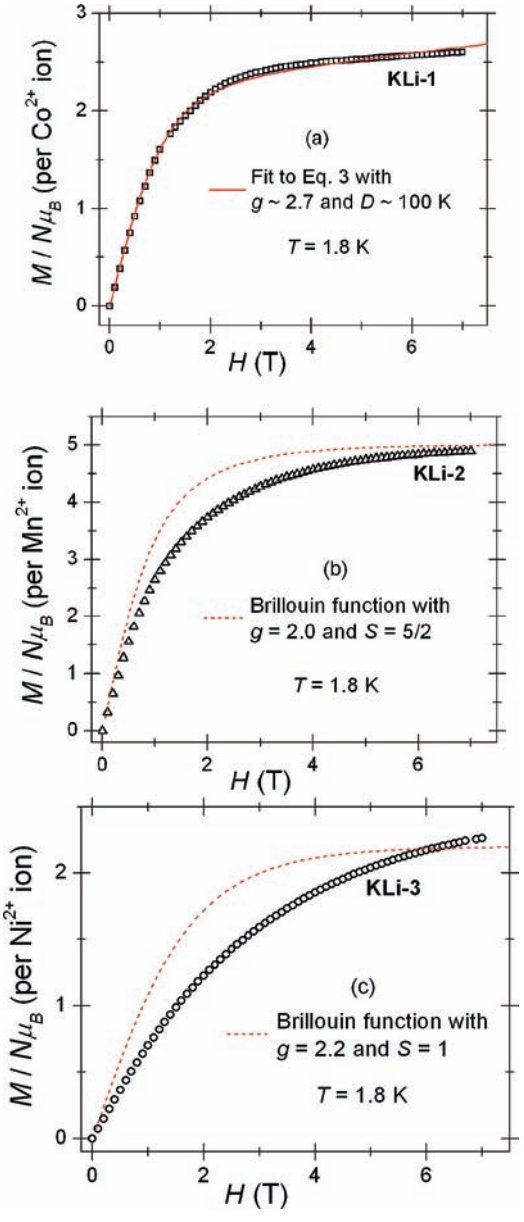

Figure 8. Magnetization as a function of field at $T = 1.8$ K for (a) **KLi-1**, (b) **KLi-2**, and (c) **KLi-3**. The solid line in (a) represents the fit to eqs 1, and the dashed lines in (b) and (c) represent Brillouin functions, respectively, for $S = 5/2$ and $S = 1$. The deviation from the Brillouin function indicates the influence of the zero-field splitting parameter D.

be seen from Figure 7, the temperature dependence of μ_{eff} for **KLi-3** can be well-described assuming isolated Ni^{2+} ions in an axial environment. Even though μ_{eff} vs T is insensitive to the sign of the zero-field splitting parameter D, in the case of **KLi-3** we found that $D < 0$ resulted in an improved fit. This implies that the $M_s = \pm 1$ levels lie lower in energy than

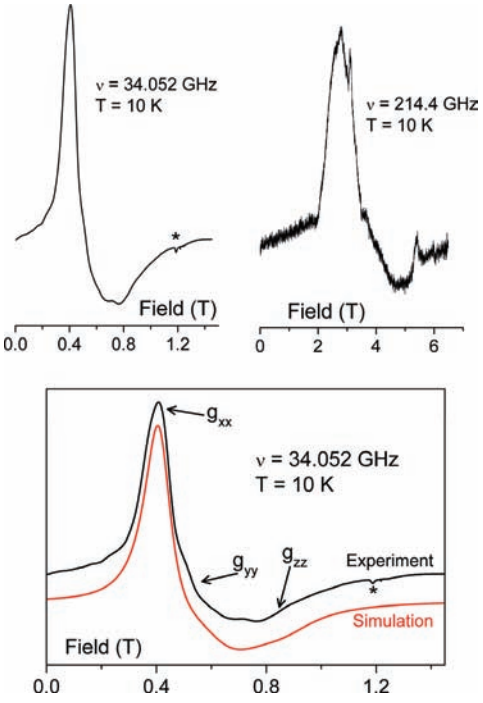

Figure 9. (a) Representative experimental EPR spectra of **KLi-1** at ~34 GHz (left) and ~214 GHz (right) at 10 K. (b) Simulated and experimental EPR spectra at ~34 GHz and 10 K. The small peak labeled with * is an impurity from the cavity.

the $M_s = 0$ level by about 8 K (see Table 2). We also observed a small antiferromagnetic interaction $\theta \sim -0.6$ K between the Ni^{2+} ions in **KLi-3** (cf. Table 2). Ni^{2+} ions in a distorted octahedral environment are known to exhibit a wide range of zero-field splitting parameters D (-9 to $+16$ K) depending on the coordinated ligands, and the observed $D \sim -8$ K for our **KLi-3** is consistent with other types of systems.[35,39−41] A considerable deviation of M vs H from a simple $S = 1$ Brillouin function (see Figure 8c) is consistent with a relatively large zero-field splitting. Detailed analysis of M vs H would require, similar to the **KLi-2** case, a numerical evaluation of eq 1 because the condition $|D| \gg g_x \mu_B H_x$ relevant for an analytical evaluation of $M_\perp$ is valid only in the low-field range since $|D| \sim 8$ K $\cong 5.5$ T. Our attempts to restrict the fit to low-field range yielded an unacceptable value for g and therefore were discarded. A further complication could be that the applied field of 7 T is not enough, unlike for **KLi-1** and **KLi-2**, to saturate the magnetization.

Electron Paramagnetic Resonance (EPR)

Powder EPR spectra of **KLi-1**, **KLi-2**, and **KLi-3** were obtained over 34−326 GHz in the temperature range 5−300 K. As a representative example of the frequency dependence

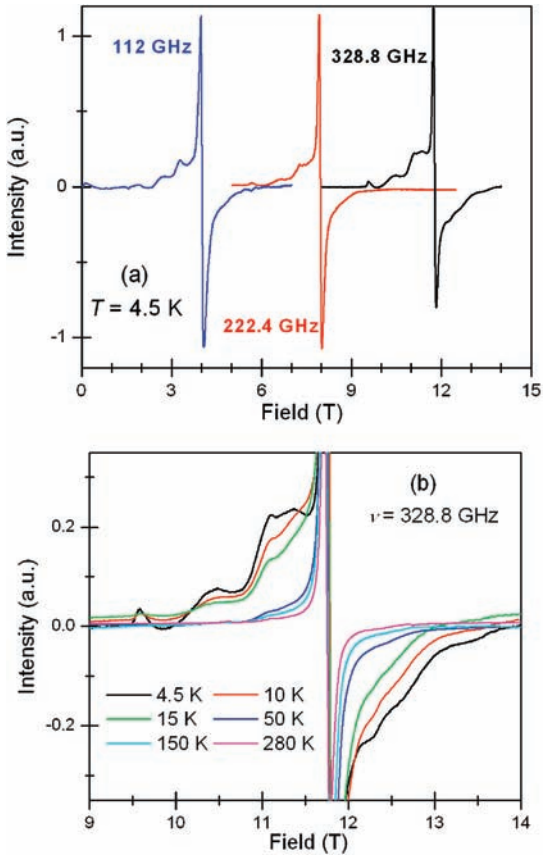

Figure 10. Representative EPR spectra of **KLi-2** showing the (a) frequency dependence at 4.5 K and (b) temperature dependence at 328.8 GHz.

of **KLi-1**, Figure 9a shows 10 K spectra at 34 and 214 GHz. Only one broad peak was observed up to frequencies of 326 GHz and fields of up to 14 T, suggesting that the zero-field splitting parameter $|D| \gg 326$ GHz, consistent with the magnetic susceptibility and magnetization data. The spectra were simulated fairly well (cf. Figure 9b) using the Hamiltonian shown in eq 3 for $S = S_{\text{eff}} = 1/2$ with the simulation parameters $g_{\text{eff},z} = 2.8 \pm 0.1$, $g_{\text{eff},y} = 4.0 \pm 0.1$, and $g_{\text{eff},x} = 5.9 \pm 0.1$. As expected[27,28] for axially distorted octahedral Co^{2+} ions, the observed isotropic g-value 4.23 is consistent with the theoretical 4.33 and the principal g-values sum up to 13.

Figure 10 shows the frequency dependence of **KLi-2** at 4.5 K and the temperature dependence at 328.8 GHz. We rule out the observed eight peaks as the hyperfine structure arising from the ^{55}Mn nucleus because of features such as the total spread (~5 T), unequal intensities, and large linewidths (~0.1 T). The spectra were reasonably simulated with the parameters $g_x = g_y = g_z = 2.06 \pm 0.01$, $D = -4800 \pm 250$ G (~0.7 K), and $E = 1000 \pm 100$ G (~0.14 K).

KLi-3 did not show any signals attributable to Ni^{2+} ions up to frequencies of 413 GHz and magnetic fields of up to 14 T. The transition $|-1\rangle \rightarrow |+1\rangle$ within the ground state becomes increasingly forbidden as the frequency/field increases. However, since $|D| \sim 155$ GHz (~ 7.5 K) when $h\nu$ exceeds $|D|M_S^2$, one expects[28a] to observe the $|-1\rangle \rightarrow |0\rangle$ transition at low temperatures and also the $|0\rangle \rightarrow |1\rangle$ transition at higher temperatures. Even though we are puzzled by the absence of these expected transitions for frequencies of up to 413 GHz, we speculate that fast spin−lattice and spin−spin relaxation processes broaden the signals beyond detection.

Conclusions

We have successfully synthesized and structurally characterized four novel transition metal containing derivatives of the cyclic 48-tungsto-8-phosphate $[H_7P_8W_{48}O_{184}]^{33-}$ (**P_8W_{48}**). The cobalt(II), manganese(II), nickel(II), and vanadium(V) containing polyanions $[Co_4(H_2O)_{16}P_8W_{48}O_{184}]^{32-}$ (**1**), $[Mn_4(H_2O)_{16}(P_8W_{48}O_{184})(WO_2(H_2O)_2)_2]^{28-}$ (**2**), $[Ni_4(H_2O)_{16}(P_8W_{48}O_{184})(WO_2(H_2O)_2)_2]^{28-}$ (**3**), and $[(VO_2)_4(P_8W_{48}O_{184})]^{36-}$ (**4**) were prepared in lithium acetate buffer medium using simple one-pot reaction conditions. Polyanions **1**−**4** exhibit four $Co^{2+}/Mn^{2+}/Ni^{2+}/V^{5+}$ ions grafted to the inner rim of the cyclic **P_8W_{48}** wheel. For polyanions **1**−**3**, these 3d metal ions are all oriented in a coplanar fashion perpendicular to the main plane of the **P_8W_{48}** host, whereas in **4** the vanadium ions occupy alternatingly up−down positions around the tungstophosphate wheel. Unexpectedly, polyanions **2** and **3** exhibit the novel $\{P_8W_{50}\}$ host framework, generated in situ by grafting of two additional equivalents of tungsten, most likely due to the presence of H_2O_2 in the reaction mixture. These octahedrally coordinated W(VI) ions are covalently bound on the inner rim of the cyclic **P_8W_{48}** wheel via two W−O(W) bonds and four terminal ligands, so that the grafted entity can be described as an all-equatorial $\{cis\text{-}WO_2(OH_2)_2\}^{2+}$ dicationic unit. This phenomenon is an important aspect of the work described here, as it indicated that perhaps derivatives of **P_8W_{48}** can be prepared with much larger tungsten content in the central cavity.

The solubility and stability conditions for **1**, **2**, and **4** were studied and allowed us to identify suitable media for their cyclic voltammetry (CV) characterization. The electroactivity of the Co^{2+} centers in **1** was unambiguously detected at pH = 5, adding a new example to the very few multicobalt POMs for which such detection was successful. In addition, the CV associated with the W-centers in **1** is sufficiently different from that of the **P_8W_{48}** precursor, allowing for distinction based on the potential locations of their respective waves. The same observations and conclusions are also valid for **2** and **4**. During a study of the Mn^{2+} centers of **2** at pH = 5, film deposition was observed to occur. The V^V centers in **4** were identified by a chemically reversible CV in a pH = 0.33 medium.

Magnetic and EPR data were collected on powder samples of **KLi-1**, **KLi-2**, and **KLi-3**. Our data is consistent with that of essentially noninteracting M^{2+} ions and the magnetic parameters obtained for each of the compounds are in reasonable agreement with the values cited in the literature.[29−41] Magnetization, magnetic susceptibility, and EPR data of **KLi-1** are consistent with the energy levels portrayed in Scheme 1c, i.e., the Co^{2+} ion has a $M_S = \pm 1/2$ ground state separated from $M_S = \pm 3/2$ by ~110−120 K. The magnetization and EPR measurements on **KLi-2** indicate that the Mn^{2+} ions have a small zero-field splitting and a fairly isotropic g-tensor, typical of octahedral, high-spin Mn^{2+} compounds.[29,36−39] The magnetic behavior of the Ni^{2+} ions in **KLi-3** is consistent[35,39−41] with that of hexacoordinated Ni^{2+} ions. **KLi-3** remains EPR silent up to 413 GHz in spite of a zero-field splitting of ~155 GHz, which we preliminarily assign to fast relaxation processes.

Finally, we would like to note that this work complements our earlier studies on transition metal ion clusters with $n = 4$,[42a] $n = 5$,[42b] and $n = 6$.[42c]

Acknowledgment. U.K. acknowledges support from the German Science Foundation (DFG KO-2288/3-2), the Fonds der Chemischen Industrie, and Jacobs University. We thank Dr. N. Izarova and Dr. M. H. Dickman for assistance with XRD. This work was supported by the CNRS and the University Paris−Sud (UMR 8000). Mrs. Wided Bellagha Chencha is thanked for preliminary stability experiments. S.N. and J.v.T. acknowledge the NSF Cooperative Agreement grants DMR-0084173 and DMR-0520481 for financial support. N.S.D. acknowledges the NSF NIRT grant no. 0506946 for partial financial support.

(42) (a) Kortz, U.; Nellutla, S.; Stowe, A. C.; Dalal, N. S.; Rauwald, U.; Danquah, W.; Ravot, D. *Inorg. Chem.* **2004**, *43*, 2308. (b) Nellutla, S.; van Tol, J.; Dalal, N. S.; Bi, L. -H.; Kortz, U.; Keita, B.; Nadjo, L.; Khitrov, G. A.; Marshall, A. G. *Inorg. Chem.* **2005**, *44*, 9795. (c) Bi, L. -H.; Kortz, U.; Nellutla, S.; Stowe, A. C.; van Tol, J.; Dalal, N. S.; Keita, B.; Nadjo, L. *Inorg. Chem.* **2005**, *44*, 896.

Supporting Information Available: X-ray crystallographic files in CIF format and additional solid state structural and solution electrochemistry information. This material is available free of charge via the Internet at http://pubs.acs.org.